Z. Phys. C 66, 385–391 (1995)

ZEITSCHRIFT
FÜR PHYSIK C

Backward proton production in π^+ and K^+ collisions with Al and Au nuclei at 250 GeV/c

EHS/NA22 Collaboration

N.M. Agababyan[h], I.V. Ajinenko[e], M.R. Atayan[h], K. Belous[e], M. Charlet[d,1], P.V. Chliapnikov[e], E.A. De Wolf[a,2], K. Dziunikowska[b,4], A.M.F. Endler[f], Z.Sh. Garutchava[g], H.R. Gulkanyan[h], R.Sh. Hakobyan[h], J.K. Karamyan[h], D. Kisielewska[b,4], W. Kittel[d], S.S. Mehrabyan[h], Z.V. Metreveli[g], L.C.S. Oliveira[f], K. Olkiewicz[b,3], F.K. Rizatdinova[c], E.K. Shabalina[c], L.N. Smirnova[c], M.D. Tabidze[g], L.A. Tikhonova[c], A.G. Tomaradze[g,4], F. Verbeure[a], S.A. Zotkin[c]

[a] Department of Physics, Universitaire Instelling Antwerpen, B-2610 Wilrijk, Belgium
[b] Institute of Physics and Nuclear Techniques of Academy of Mining and Metallurgy and Institute of Nuclear Physics, PL-30055 Krakow, Poland
[c] Nuclear Physics Institute, Moscow State University, RU-119899 Moscow, Russia
[d] University of Nijmegen/NIKHEF, NL-6525 ED Nijmegen, The Netherlands
[e] Institute for High Energy Physics, RU-142284 Protvino, Russia
[f] Centro Brasileiro de Pesquisas Fisicas, BR-22290 Rio de Janeiro, Brazil
[g] Institute for High Energy Physics of Tbilisi State University, GE-380086 Tbilisi, Georgia
[h] Institute of Physics, AM-375036 Yerevan, Armenia

Received: 21 November 1994

Abstract. Backward proton production is studied in interactions of π^+ and K^+ mesons with Al and Au nuclei at 250 GeV/c. The proton momentum spectra are measured at different emission angles. From the two-proton correlations, it is found, that a significant part ((26±4)% for Al and (44±6)% for Au) of the backward proton production can be attributed to secondary pion absorption by a nucleon pair in the nuclear medium, $\pi^+(pn) \to \overleftarrow{p}\,p$ and $\pi^0(pp) \to \overleftarrow{p}\,p$. It is found that the share of the secondary pion absorption can be fitted by a power dependence $\propto A^{\beta}$, with $\beta = 0.27 \pm 0.05$. An upper limit of the cross section for the colour-charge-exchange mechanism of backward proton production is estimated.

1 Introduction

Backward proton production (BPP) is kinematically forbidden in the lab. frame if the interaction takes place on a free nucleon. Selecting on backward protons, one therefore can select processes in which two or more nucleons of the nucleus are involved. Two classes of these processes can be distinguished. The first one is a "direct" (spectator type) mechanism of projectile collision with two (or more) nucleons or multiquark compositions in the nucleus (see e.g. [1,2]). The contribution of this mechanism has experimentally been estimated for νNe and $\bar{\nu}Ne$ -interactions and found to be (25±8)% and (17±8)%, respectively [3]. The second class are two (or multi)-step mechanisms of secondary intranuclear collisions (see e.g. [4,5]).

One of the simplest two-step mechanisms of BPP is the absorption of a low-energy secondary pion (SPA) by a pair of nucleons in a nucleus, $\pi NN \to \overleftarrow{p}\,N$. As recently observed in collisions of hadrons with light nuclei (carbon, neon) [6-8], the contribution of SPA to BPP with momenta $p_{lab} > 0.2 - 0.25$ GeV/c is significant ($20 - 25\%$). Up to now, no experimental results exist for heavy nuclei, except for an indication obtained in neutrino interactions with freon (CF_3Br) [9].

As another interesting multi-step mechanism of BPP, double colour-charge exchange (CCE) has been proposed in [10,11] for diffractive-like hadron-nucleus interactions. A possible observation of CCE has been reported recently in $\pi^- Be$ interactions at 40 GeV/c [12], but further experimental investigations are necessary.

A third multi-step contribution to BPP is secondary elastic rescattering. As theoretically estimated (see e.g. refs. [4,5] and references therein), it can play a significant role in BPP. However, the estimates of the absolute yield of backward protons suffers large uncertainties.

In this paper, we present results on BPP in interactions of π^+ and K^+-mesons with Al and Au nuclei at 250 GeV/c from the NA22 experiment, performed at the CERN SPS with the help of the European Hybrid Spectrometer EHS. The experimental procedure is described in the following section. The multiplicity distribution of backward protons and their inclusive spectra in different angular intervals are presented in Sects. 3 and 4. Particular mechanisms of BPP are considered in Sect. 5. Conclusions are summarized in Sect. 6.

[1] EC guest scientist, now at DESY, Hamburg
[2] Onderzoeksleider NFWO, Belgium
[3] Supported by the Polish State Committee for Scientific Research
[4] Now at UIA, Wilrijk, Belgium

2 Experimental procedure

The experimental set-up of EHS is described in detail in [13], the data reduction procedure in [14-16]. A rapid cycling bubble chamber RCBC, 80 cm in diameter and filled with hydrogen, was used as vertex and track detector, as well as an ionization device. A 2T magnetic field was applied along the cylinder axis. The RCBC was equipped with two nuclear targets consisting of an aluminium and a gold foil of thickness 2.5 mm and 0.64 mm, respectively, corresponding to 0.5 % of an interaction length. The foils were placed side by side, orthogonally to the beam, 15.5 cm behind the entrance window of the chamber.

Tracks of secondary charged particles, leaving RCBC through the exit window, are reconstructed from hits in the wire and drift chambers of the spectrometer and from measurement in RCBC. The backward tracks (i.e. tracks with a lab. frame production angle $\theta_{lab} > 90^0$) are reconstructed from measurement in RCBC. The average momentum resolution for charged particles varies from 1 to 2% for tracks reconstructed in the bubble chamber and from 1 to 2.5% for those reconstucted in the spectrometer. For reconstructed tracks with lab momentum $p_{lab} < 1.2$ GeV/c, the ionization strength was estimated visually on the scanning table.

The following selection criteria are used for the events (see details in [16,17]): the interaction vertex is within one of the nuclear foils; the event is satisfactorily measured and reconstructed and is not a candidate for a quasi-elastic or coherent interaction with the nucleus. The events are weighted with a multiplicity dependent weight in order to compensate for the loss of events due to badly reconstructed tracks. The numbers of accepted events are 1046 K^+Al, 897 K^+Au, 3420 π^+Al and 2816 π^+Au events.

In order to select BPP events, we further use the following procedure:

a) For tracks with ionization compatible with the proton hypothesis, *stopping* in the liquid hydrogen of RCBC, a momentum measurement exists from the track curvature and a range measurement from the endpoint (for details see [18]). The relation between momentum p_{curv} (in GeV/c) and range l (in cm),

$$R = 0.96194 \log_{10} p_{curv} - 0.27328 \log_{10} l \quad , \qquad (1)$$

is expected to give $R = -0.82$ for protons, -0.61 for deuterons, -0.50 for tritons and -0.25 for α-particles. The distribution in R for positive stopping tracks with ionization compatible with the proton hypothesis, $(\Delta p/p)_{curv} < 0.3$ and production angle in the full angular interval $0^0 \leq \theta_{lab} \leq 180^0$ is shown in Fig. 1a. The proton and deuteron peaks are clearly seen. Tracks with $R < -0.69$ are accepted as proton (see also [18]). The corresponding distribution for tracks with $\theta_{lab} > 90^0$ is shown in Fig. 1b. Also here, the cut $R < -0.69$ is applied to define protons.

b) For tracks with ionization compatible with the proton hypothesis, but *leaving* the fiducial volume, we check the consistency between the measured path l of the track in RCBC and its measured momentum p_{curv} for the proton hypotheses. We accept a track as a proton if the potential path calculated for a proton with momentum $p = (p + \Delta p)_{curv}$ in hydrogen exceeds l. (This limit is used, in order to avoid proton losses due to momentum resolution).

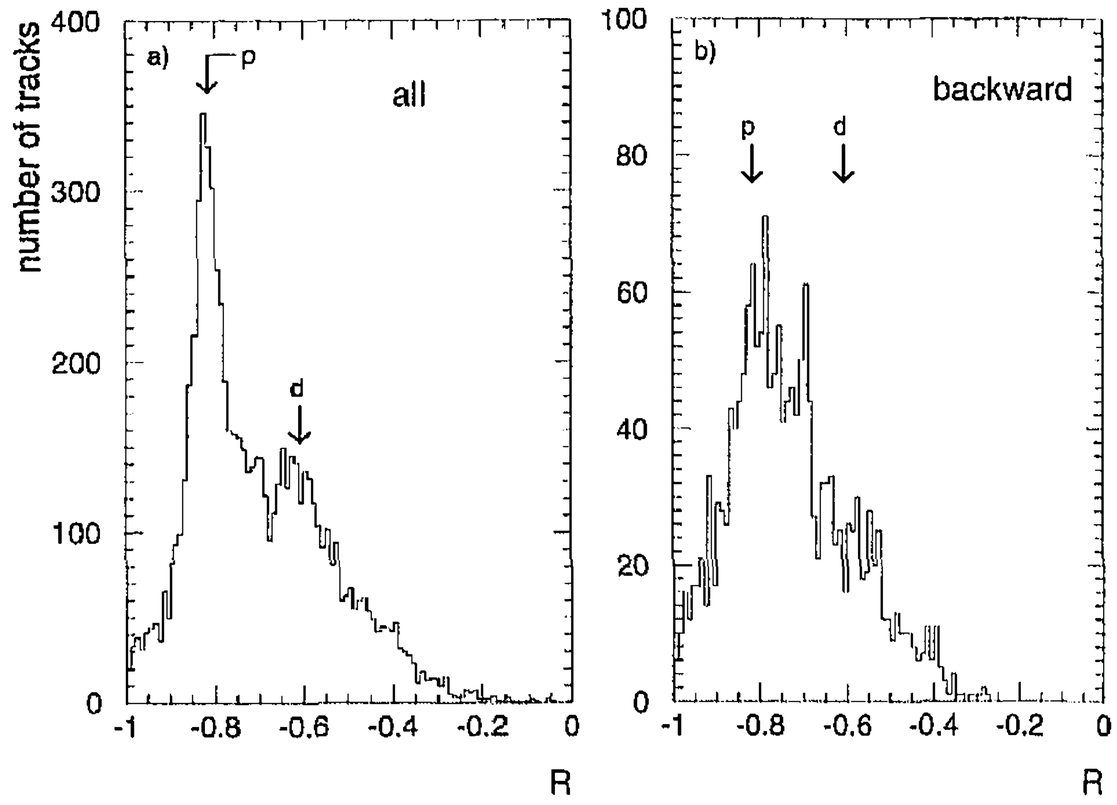

Fig. 1. Distribution in R (see definition in the text) of positive stopping tracks for the combined sample of M^+Al and M^+Au events **a**) for all tracks, **b**) for backward tracks

Table 1. The total number of events N^{ev}_{tot}, the number of events with backward protons $N^{ev}_{\overleftarrow{p}}$, the number of backward protons $n_{\overleftarrow{p}}$ and $\langle n_{\overleftarrow{p}} \rangle$ the average number of backward protons with $\theta_{lab} \geq 100^0$ and $p_{lab} > 0.24$ GeV/c

interaction	N^{ev}_{tot}	$N^{ev}_{\overleftarrow{p}}$	$n_{\overleftarrow{p}}$	$\langle n_{\overleftarrow{p}} \rangle$
M^+Al	4466	596	678	0.159 ± 0.006
M^+Au	3713	1189	2061	0.640 ± 0.016

At the relatively large momenta of $p_{lab} > 0.5$ GeV/c of backward tracks, some contamination is possible from misidentified π^+ mesons and from deuterons. From the available high-energy data [19] on backward $\pi^\pm$ meson production off nuclear targets, and from our measurement of the backward produced particles (see Sect. 4 below), the contamination from π^+ mesons is found to be negligible. The contamination of the proton sample at $p_{lab} > 0.5$ GeV/c by deuterons is, however, estimated to about 20% [20].

In the relatively low-momentum region of $p_{lab} < 0.5$ GeV/c, the proton momenta are corrected for ionization losses in the nuclear foils (see also [17]). In the further analysis, we exclude protons with $p_{lab} < 0.24$ GeV/c (kinetic energy $T \approx 0.03$ GeV), since these can mainly be attributed to nuclear "evaporation" products. (We have checked that varying this limit to $p_{lab} = 0.274$ GeV/c ($T = 0.04$ GeV) does not change the results beyond errors.)

c) We further exclude protons with polar angle $90^0 < \theta_{lab} < 100^0$, in order to avoid large correction for losses due to bad reconstruction of protons at $\theta_{lab} \sim 90^0$.

Since we do not observe any significant difference between the π^+ and K^+ samples, we enhance the statistical significance by presenting the combined sample of π^+ and K^+ collisions. This sample will be denoted as "M^+" collisions. The total number of events, the number of accepted BPP events and the total number of accepted backward protons and their average per event are presented in Table 1, separately for M^+Al and M^+Au collisions.

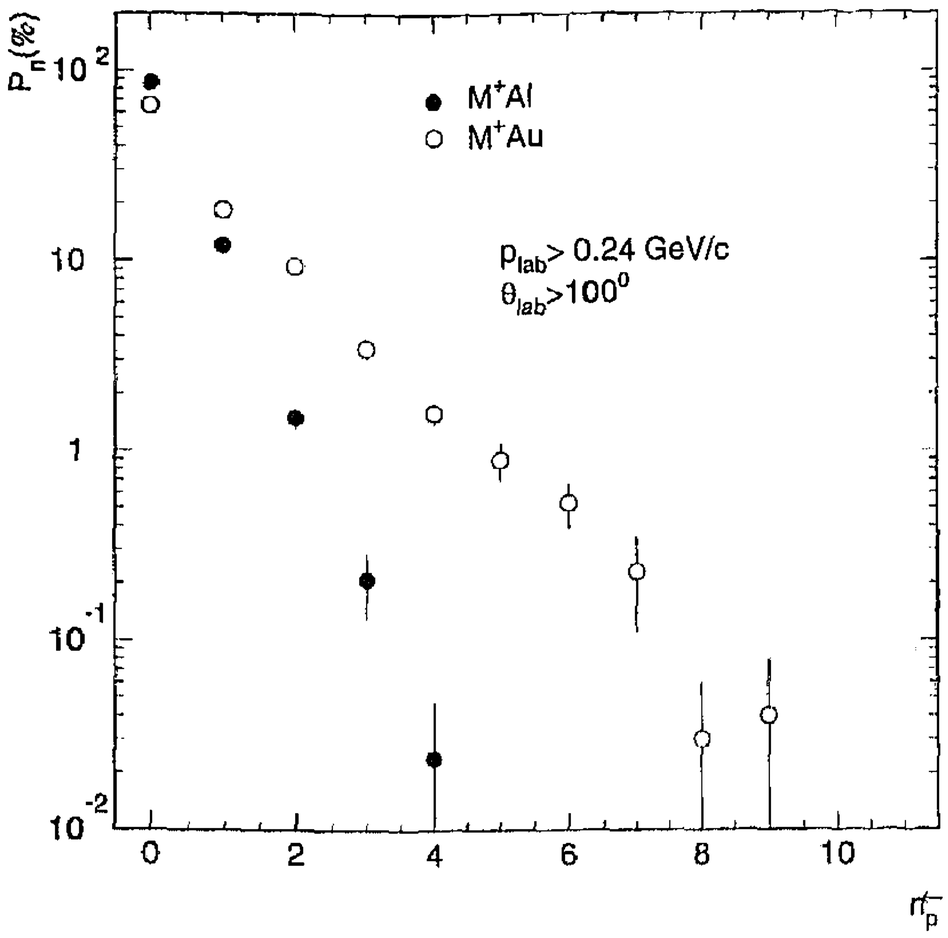

Fig. 2. The multiplicity distribution for backward protons, with $p_{lab} > 0.24$ GeV/c and $\theta_{lab} \geq 100^0$ in M^+Al and M^+Au interactions

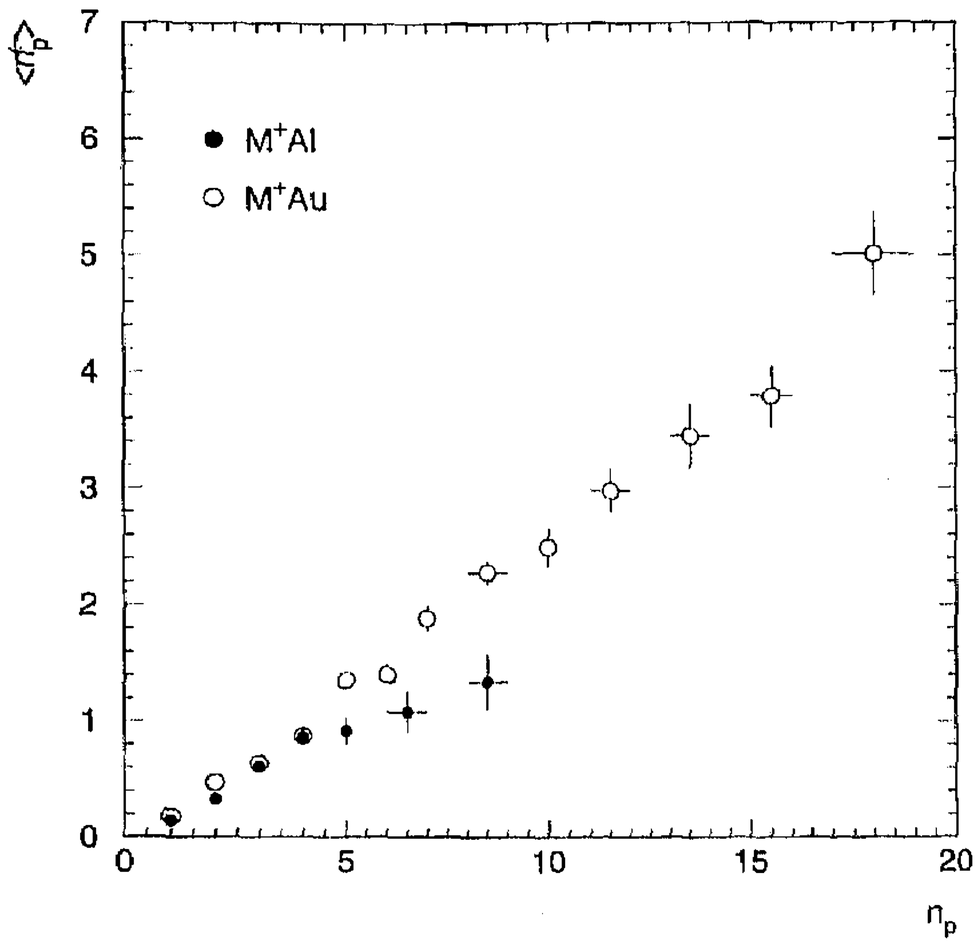

Fig. 3. The average multiplicity of protons emitted with $\theta_{lab} \geq 100^0$, as a function of the total number of protons, in M^+Al and M^+Au interactions

3 The multiplicity distribution of backward protons

In Fig. 2, we show the multiplicity distribution for protons with $p_{lab} > 0.24$ GeV/c and $\theta_{lab} > 100^0$, both for M^+Al and M^+Au interactions. Assuming a power dependence of the backward proton yield $\langle n_{\overleftarrow{p}} \rangle$ (Table 1) as a function of the mass number A, $\langle n_{\overleftarrow{p}} \rangle \propto A^\alpha$, we obtain $\alpha = 0.70 \pm 0.03$.

As one can see from Fig. 3, the average multiplicity $\langle n_{\overleftarrow{p}} \rangle$ of backward protons increases (for Au almost linearly) with increasing multiplicity of all protons n_p. A similar dependence has been observed for the (lighter) nucleus in pNe-interactions at 300 GeV/c [8].

4 The inclusive spectra of backward protons

The normalized invariant inclusive backward-proton cross section per nucleon of BPP, $(1/\sigma_{in})\ (E/A) d^3\sigma/dp^3$, is presented as a function of p_{lab} (full circles) in Figs. 4 and 5 for different angular intervals in M^+Al and M^+Au interactions, respectively. Our results are in reasonable agreement with data obtained at fixed angles in pAl and pTa interactions at 400 GeV/c [20] (open circles), if one takes into account the 20% normalization uncertainty quoted for the latter.

The π^+ mass is assigned to a track if its ionization is compatible with the pion hypothesis and the proton hypothesis is not compatible with either ionization or momentum-path relation. The resulting backward- π^+ cross section is shown as full triangles in Figs. 4 and 5 and is also in agree-

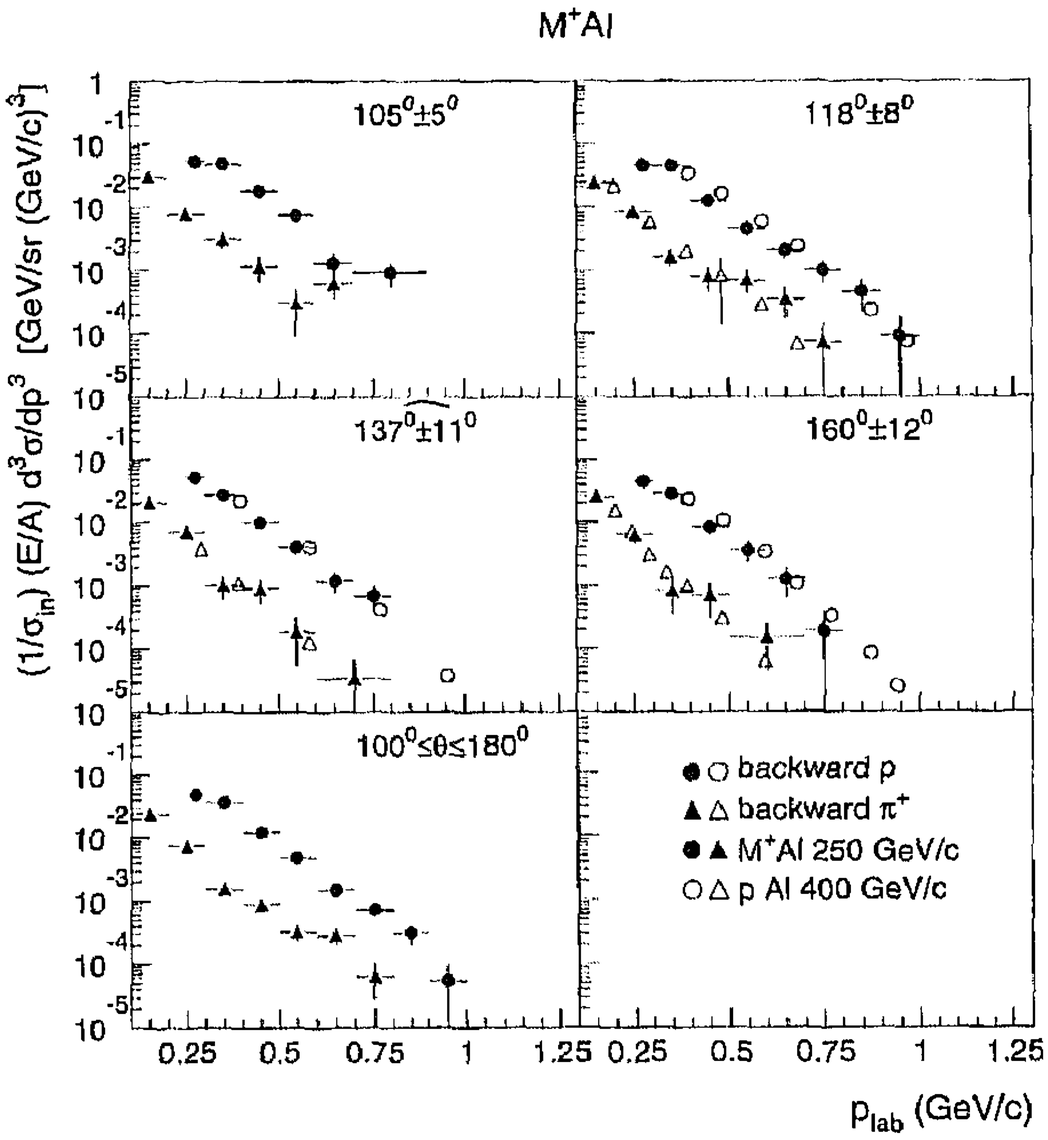

Fig. 4. The normalized invariant inclusive cross section per nucleon for backward protons and π^+ mesons in different angular ranges, as a function of p_{lab}, for M^+Al interactions

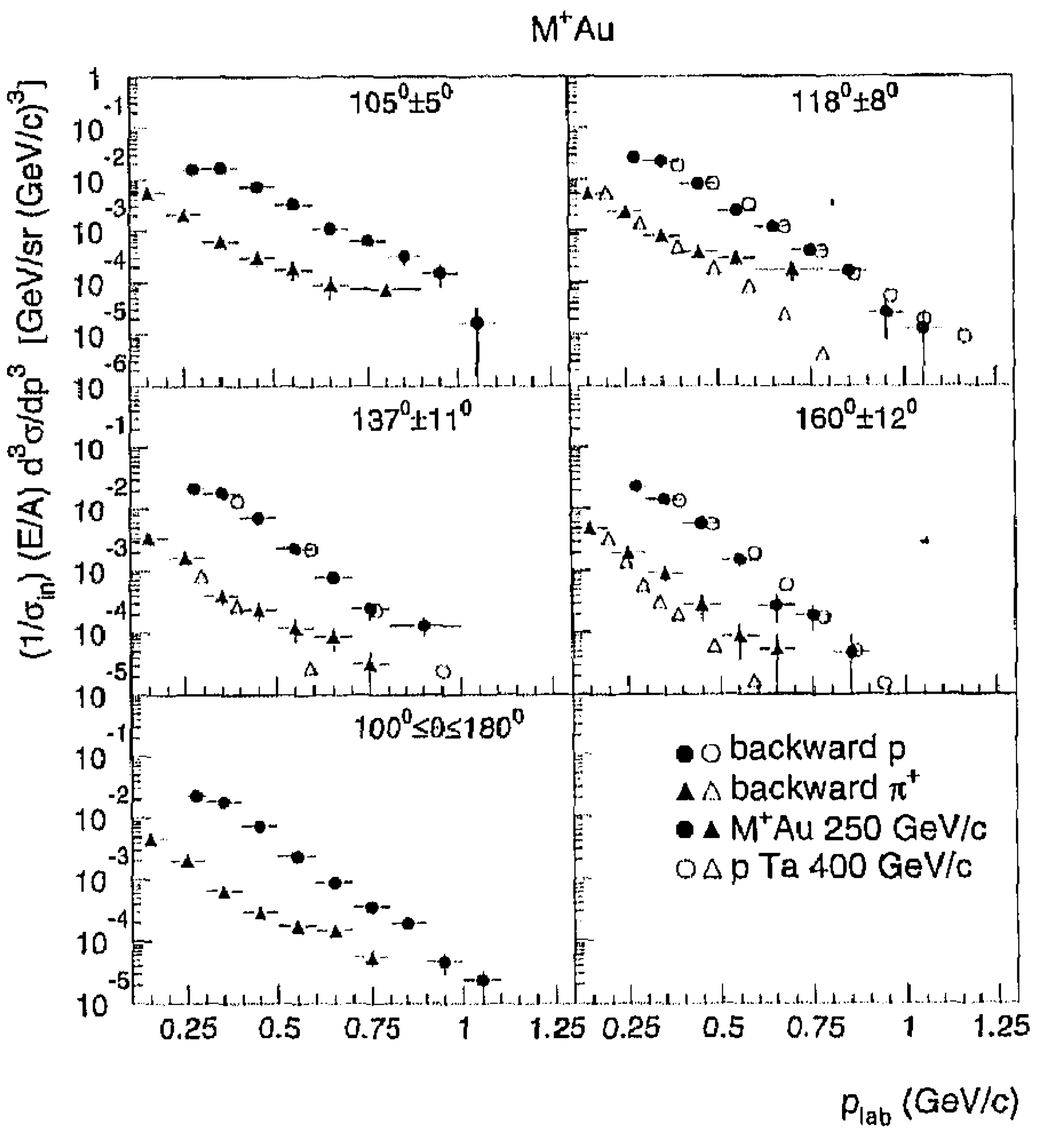

Fig. 5. The same as Fig. 4, but for M^+Au interactions

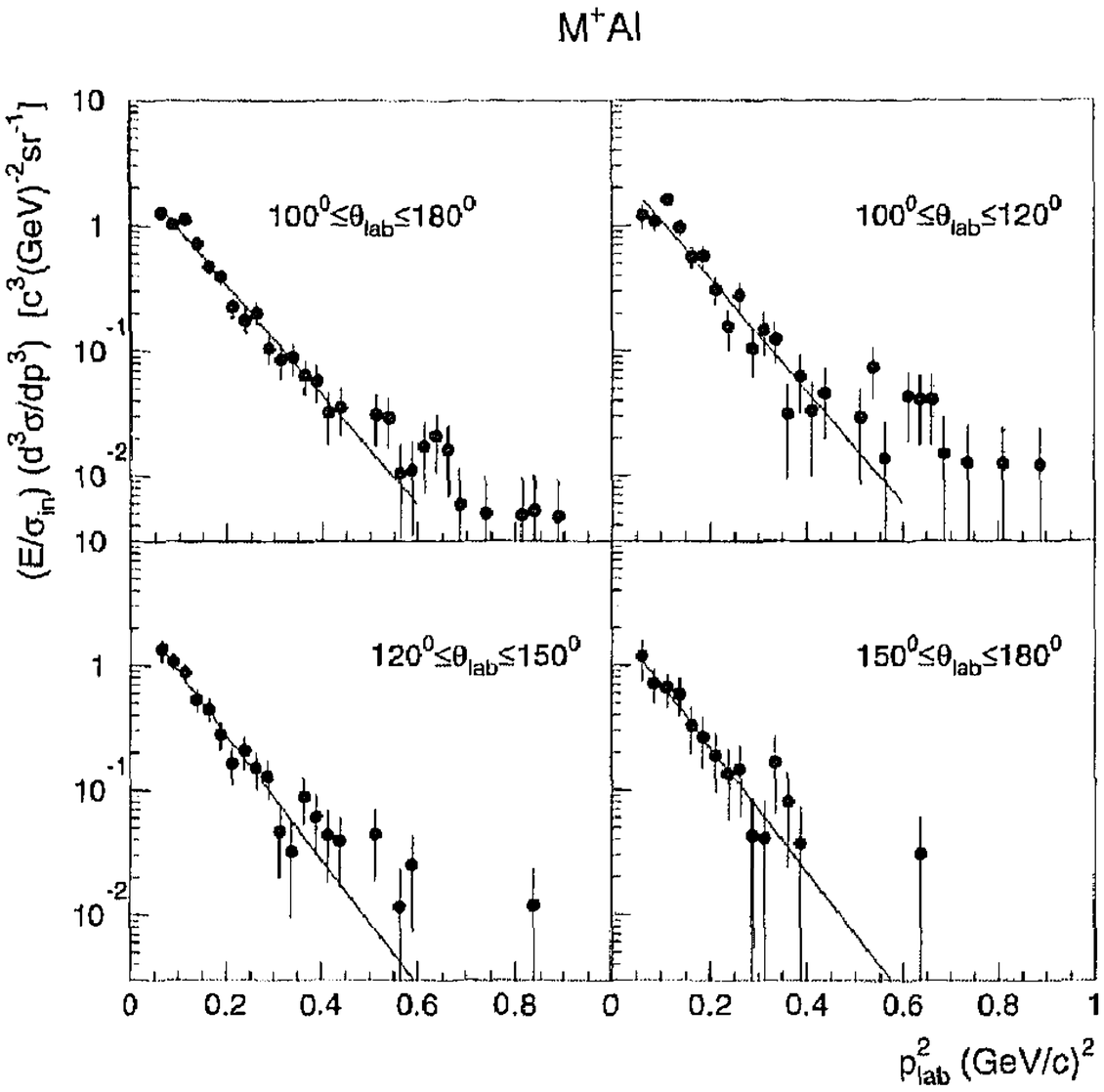

Fig. 6. The normalized invariant inclusive cross sections for backward protons in different angular ranges, as a function of p^2_{lab}, for M^+Al interactions. The curves correspond to the best exponential fit in the range $0.0625 < p^2_{lab} < 0.6$ GeV/c

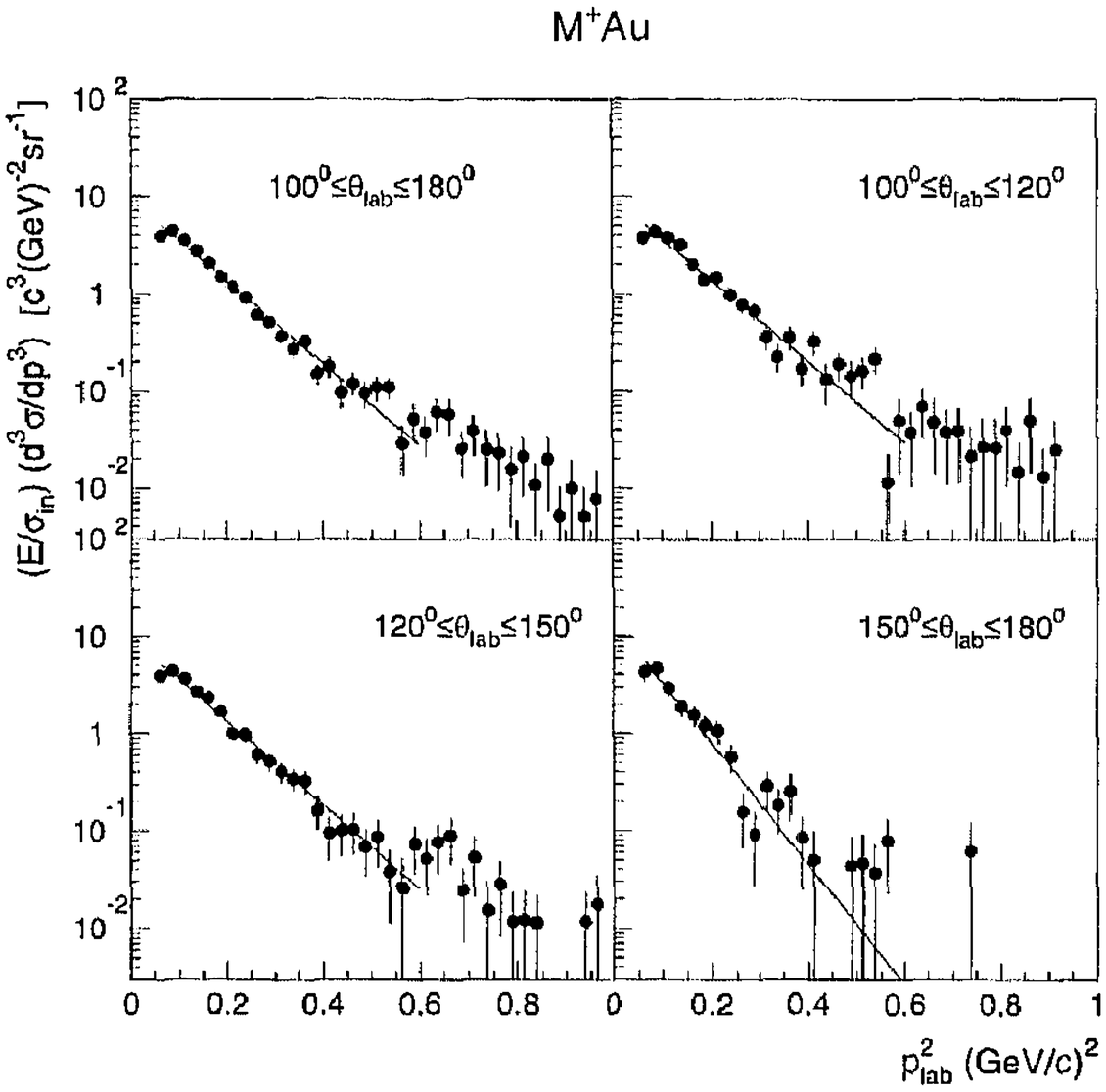

Fig. 7. The same as Fig. 8, but for M^+Au interactions

ment with available high-energy data obtained in pAl and pTa interactions at 400 GeV/c [19] (open triangles). Our π^+ data for Au are somewhat higher than those for Ta in [19], i.e. part of our protons may be misidentified as pions at $p_{lab} > 0.5$ GeV/c. However, because of the large difference in relative yield, the consequent underestimate of the proton data is smaller than the statistical errors of our proton data.

The normalized invariant cross section $(E/\sigma_{in})d^3\sigma/dp^3$ is shown in Figs. 6 and 7 as a function of p^2_{lab} for different angular intervals. In the region $0.0625 < p^2_{lab} < 0.6$ (GeV/c)^2 the spectra can be described by the conven-

Table 2. Fit results for the exponential behavior of the p^2_{lab} spectra of Figs. 6 and 7 for $0.0625 < p^2_{lab} < 0.6$ (GeV/c)^2

target	θ	a(GeV^{-1}c$^2sr^{-1}$)	b (GeV/c)$^{-2}$	χ^2/NDF
Al	$100^0 \div 120^0$	3.1 ± 0.5	10.4 ± 0.8	41/24
Al	$120^0 \div 150^0$	2.8 ± 0.6	11.5 ± 1.1	15/18
Al	$150^0 \div 180^0$	2.3 ± 0.8	11.5 ± 2.1	5/13
Al	$100^0 \div 180^0$	2.6 ± 0.3	10.2 ± 0.6	30/26
Au	$100^0 \div 120^0$	9.7 ± 0.8	9.7 ± 0.4	54/33
Au	$120^0 \div 150^0$	9.8 ± 0.8	9.9 ± 0.4	32/32
Au	$150^0 \div 180^0$	13.8 ± 2.6	14.3 ± 1.2	22/18
Au	$100^0 \div 180^0$	9.3 ± 0.6	9.7 ± 0.3	60/35

tional exponential form $a\exp(-bp^2_{lab})$. Fit results are given in Table 2. The slope parameter b is, within errors, independent of the mass number A, but for Au there is an indication for an increase with increasing emission angle θ_{lab}. This behaviour and the magnitude of the slope parameter are in agreement with the results of other experiments in the wide incident energy region from a few GeV to a few hundred GeV performed with hadrons (see [8,20,21] and refs. therein), neutrinos (see [3,22] and refs. therein) and photons (see [23,24] and refs. therein).

5 Mechanisms of backward proton production

5.1 Coulour charge exchange

An interesting multi-step mechanism for BPP in hadron-nucleus interactions has been proposed by Kopeliovich and Nidermayer [9,10]. The incident hadron exchanges colour (by gluon exchange) consecutively with two nucleons in a nucleus and becomes white again. A colour flux tube is stretched between the two coloured "nucleons". As a result, one of them acquires a momentum directed backward. This process is similar to beam diffraction (elastic or inelastic). The colour charge exchange (CCE) model predicts that the momentum spectrum of the backward proton should be harder than in inclusive BPP and should have a maximum at p_{lab}~500 to 600 MeV/c.

In order to look for CCE, we select diffractive-like events

$$M^+ + A \longrightarrow \overleftarrow{p} + M^* + A' \qquad (2)$$

with at least one backward proton, no particle produced in the target fragmentation region (except for recoil protons with $p_{lab} < 1.2$ GeV/c and other nuclear fragments labelled A') and only fast products (with rapidity $y^* > 0$ in the meson-nucleon c.m.) from the fragmentation of the excited mesonic state M^* (the summed charge of which is required to be Q=+1). Note, that in the CCE mechanism the second (forward going) nucleon can acquire a relatively large momentum (2 to 4 GeV/c). Since these events are not accepted by our selection criteria, our accepted sample favours the CCE mechanism in which a (pn)-pair is involved, with a forward going neutron not detected in our experiment.

Fig. 8 shows the backward-proton momentum-distributions for reactions (2) (shaded histograms), compared to the

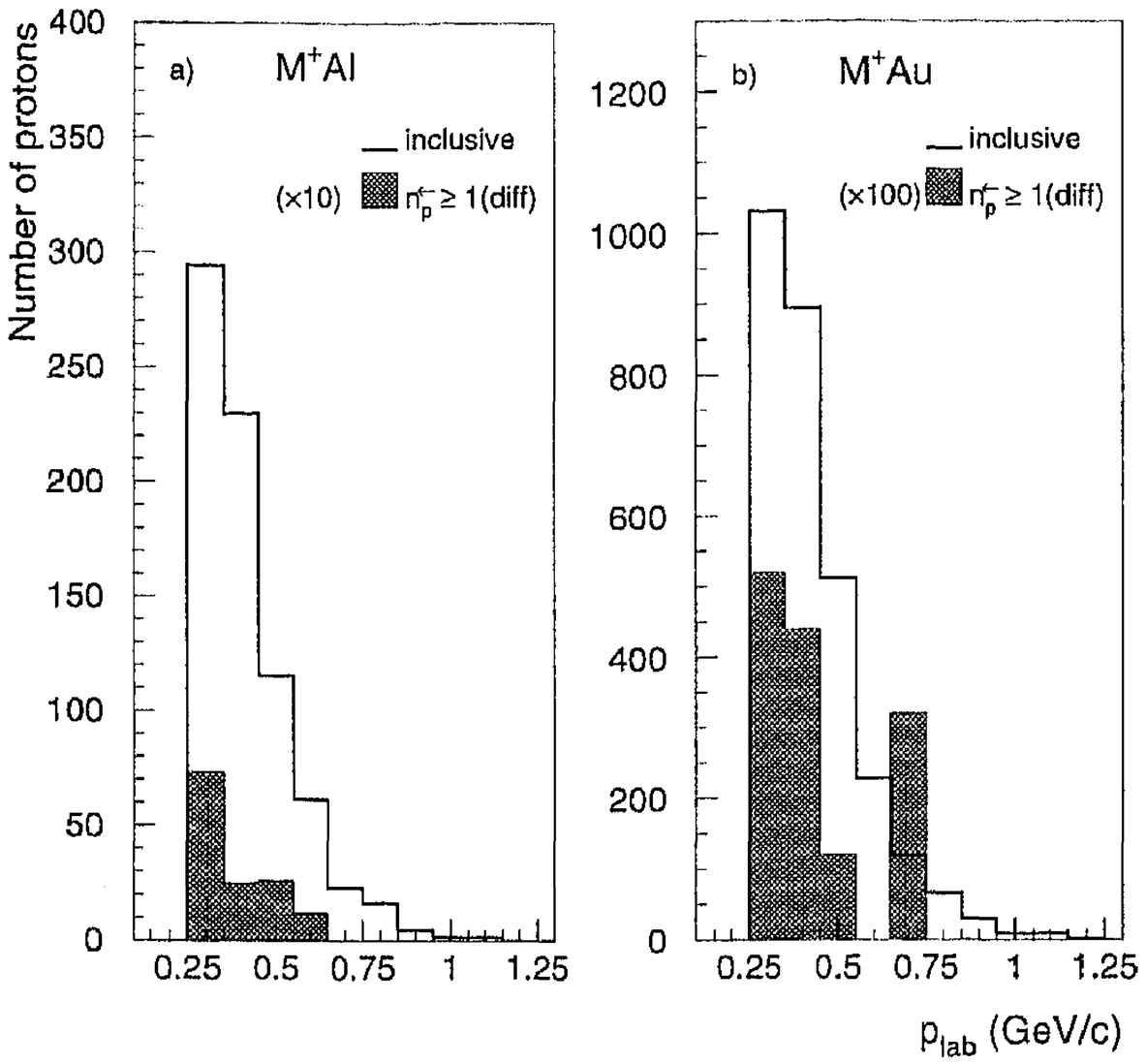

Fig. 8. The momentum distribution of backward protons in reaction (2)

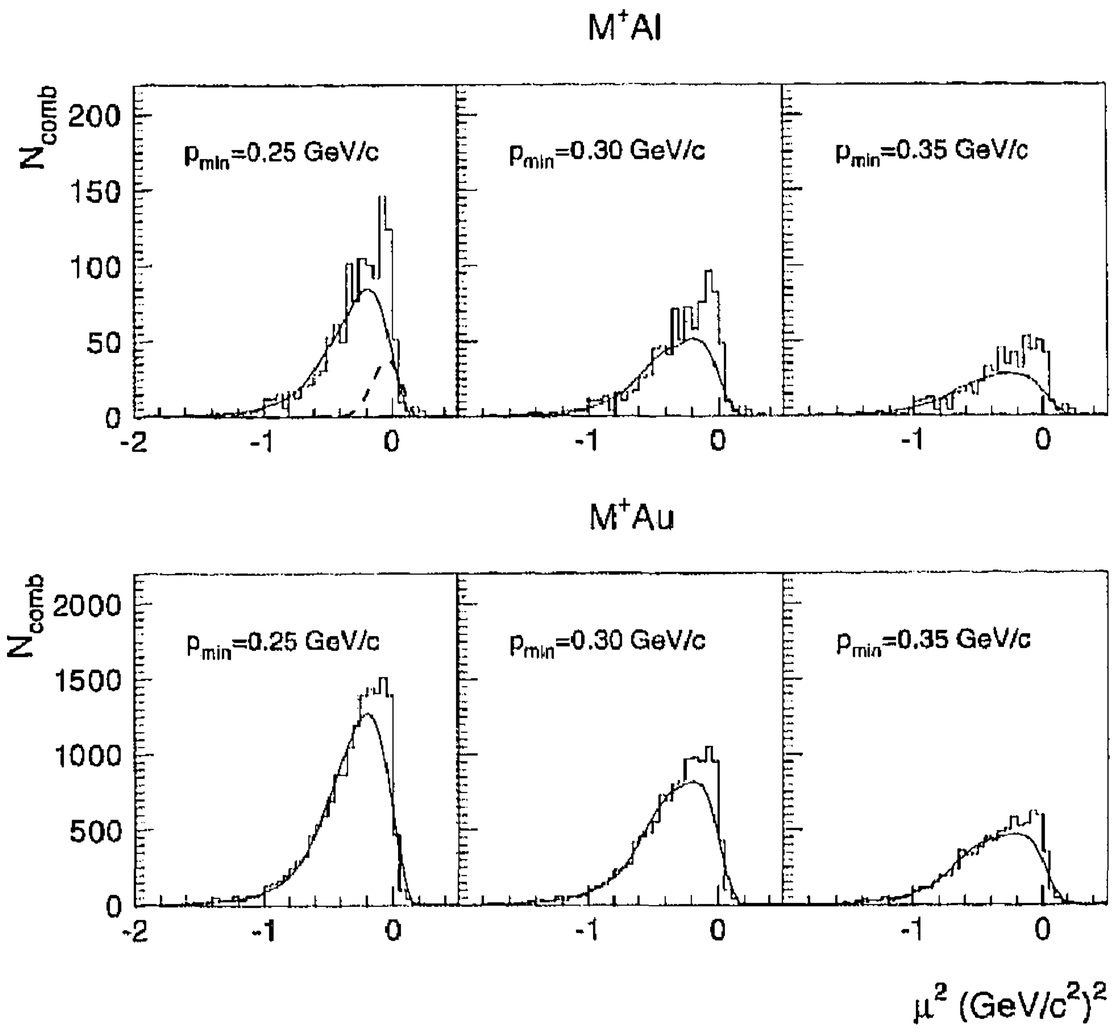

Fig. 9. The distribution in μ^2 at different p_{min} values. The solid curves refer to the background and the dashed curve demonstrates the result of the Monte Carlo simulation of subprocess (3) for Al (see text)

inclusive BPP distribution (line histogram, note the factor 10 in scale for Fig. 8a and 100 for Fig. 8b). The cross section for the semi-inclusive reactions (2) as obtained by counting the number of protons in the shaded area is 0.8±0.3 mb for Al and 3.8±1.2 mb for Au, respectively. In spite of the acceptance loss described above, these values must be considered an *upper* limit for the CCE cross section:

The Au data may indicate some possible hardening with respect to the inclusive spectrum of BPP at $p_{lab} >$ 0.55 GeV/c, as would be expected for the CCE spectrum (Fig. 8b). Even assuming that this hardening is real and can be fully attributed to CCE, we reduce the upper limit of its cross section to $\sigma_{Au}^{CCE} = 0.8 \pm 0.6$ mb, which is less than 1% of the high-momentum tail ($p_{lab} > 0.55$ GeV/c) of the inclusive spectrum. This is in contradiction with the expectation that CCE dominates in high-momentum BPP. However, within the semi-inclusive reaction (2) the contribution of CCE can achieve up to $\sim$ 10% for M^+Al and $\sim$ 20% for M^+Au interactions (see shaded histograms in Fig. 8). These rough estimates are not in contradiction with results reported in [12].

5.2 Secondary pion absorption

Another multi-step mechanism of BPP is the absorption of a secondary pion, SPA, on a correlated nucleon pair or quasi-deuteron within the nucleus,

$$\pi(NN) \longrightarrow \overleftarrow{p}\, p \quad . \tag{3}$$

The momentum dependence of the cross section for π^+ scattering on a free deuteron, $\sigma_a(\pi^+ d \rightarrow pp)$, has resonance character with a maximum of $\sigma_a \approx$12mb at $p_\pi \sim$0.25 GeV/c, dropping to $\sim$4mb at 0.5 GeV/c and $\sim$2mb at 0.75 GeV/c [25]. Therefore, one can expect that, in the SPA mechanism, the dominant role is that of low-energy secondary pions (with $p_\pi < 0.5$ GeV/c).

In order to search for the SPA mechanism, we use the method of kinematical analysis proposed in [6,7]. As a variable describing the kinematical correlation of the secondary protons in subprocess (3) we use

$$\mu^2 = (T_1 + T_2)^2 - (\mathbf{p}_1 + \mathbf{p}_2)^2, \tag{4}$$

where T_1, T_2 and $\mathbf{p_1}, \mathbf{p_2}$ are the kinetic energies and momenta of the secondary protons. For the reaction on a free deuteron, $\pi^+ d \longrightarrow pp$, the relation $\mu^2 \equiv m_\pi^2$ would hold. One can show that the binding of the nucleon pair in the nucleus and its Fermi motion lead to a shift of the peak in the μ^2 distribution from $\mu^2 = m_\pi^2$ towards smaller values by a quantity $\delta \approx 2\Delta E(T_1 + T_2) - p_d^2$ and to its broadening by $\gamma \approx \pm 2|\mathbf{p_d}(\mathbf{p_1}+\mathbf{p_2})|$, where ΔE is the average binding energy of the nucleon pair and p_d is the average magnitude of its Fermi momentum.

We look for the SPA mechanism in the reaction

$$M^+ + A \longrightarrow \overleftarrow{p} + p + X, \tag{5}$$

where the second proton can be produced either in the forward or backward direction. Note, that in subprocess (3) on a free deuteron, the minimal momentum of a secondary proton would be $p_{min} = 0.37$ GeV/c. However, due to the Fermi motion of the nuclear pair (NN) in the nucleus, this boundary can decrease to 0.2 GeV/c. In the selection of our sample for reaction (5) we, therefore, vary p_{min} from 0.25 to 0.35 GeV/c.

Furthermore, it should be taken into account that rescattering of secondary protons in the nuclear matter would result in an additional broadening of the distribution, mainly towards smaller values of μ^2. While the protons diverge at large angles in subprocess (3), rescattering preferably leads to a decrease in the angle between protons, i.e. to a decrease in μ^2.

The histograms in Fig. 9 show the μ^2 distribution for reaction (5) with $p_{min} = 0.25, 0.30$ and 0.35 GeV/c, respectively. The full curves correspond to a *"background"*

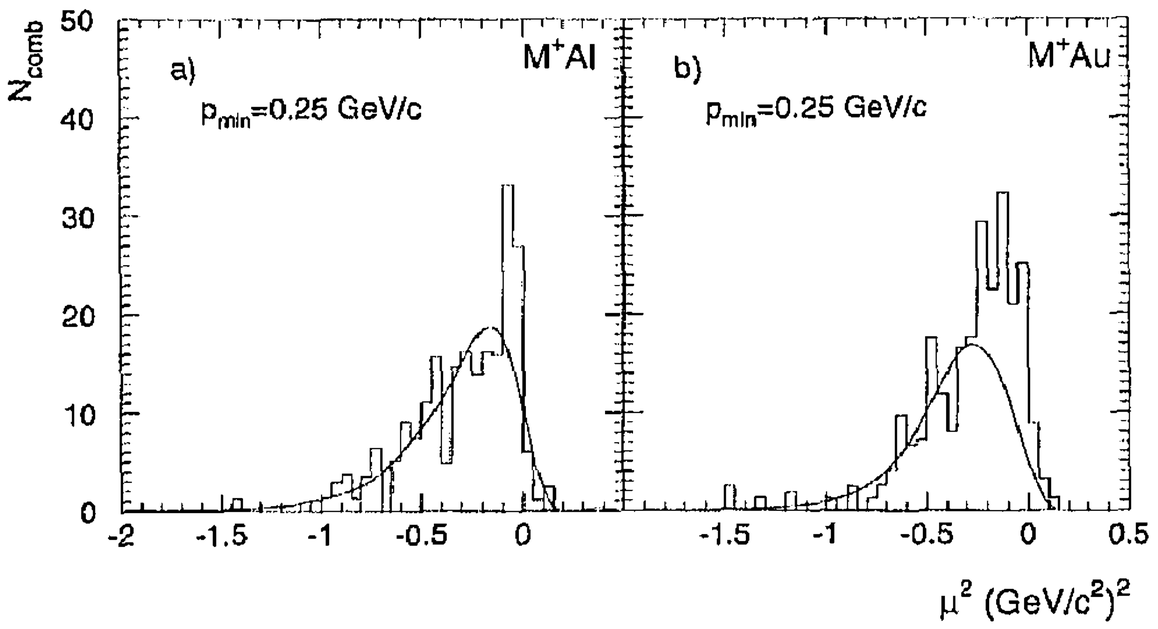

Fig. 10. Distribution in μ^2 for events with one pair of protons a) for M^+Al and b) for M^+Au interactions. The curves refer to the background (see text)

distribution, obtained by combining protons randomly chosen from different events and normalized to the experimental distribution in the region $\mu^2 < -0.25$ (GeV/c^2)^2 where the contribution of mechanism (3) is expected to be negligible.

The dashed curve in Fig. 9a demonstrates the result of a Monte Carlo simulation of subprocess (3) for Al. The following values are used : $\Delta E = 60$ MeV [26] and $\langle p_d^2 \rangle = (220$ MeV/c$)^2$ [27]. The momentum dependence of the total and differential cross section of (3) is taken from [25,28,29]. The shape of the simulation is almost insensitive to the momentum of the "incident" pion of (3). Nevertheless, the pion momentum is simulated in the range $p_\pi < 0.9$ GeV/c according to the π^+ meson spectrum obtained from our M^+Al data. The experimental error in measurement of the final proton momentum ($\langle \Delta p/p \rangle = 2\%$) is also taken into account. This simulated μ^2-distribution has a peak shifted from $\mu^2 = m_\pi^2$ to the left by about 0.1 (GeV/c^2)^2 and a tail falling below 5% of the total content at $\mu^2 \approx -0.25$ (GeV/c^2)^2. The dashed line is normalized to the difference between histogram and solid line of Fig. 9a in the region $\mu^2 > -0.25$ (GeV/c^2)^2. One can see that after subtraction of the background distribution (full line) from the histogram, the shape of the resulting distribution would be similar to that of the simulated one (dashed).

Fig. 10 shows the μ^2 distribution for $p_{min} = 0.25$ GeV/c for the subsample with a *single* pair of protons. The latter corresponds to more peripheral collisions for which the contribution from secondary interactions is less than for the full sample. As expected for the SPA mechanism, the μ^2 - distribution for the single proton pair (Fig. 10) is narrower than that for the full sample (Fig. 9).

The number of combinations in Fig. 9 and 10 above background at $\mu^2 > -0.25$ (GeV/c^2)^2 is used as an estimate of the contribution of the SPA mechanism to inclusive BPP, $r = \sigma^{SPA}(\overleftarrow{p}\,p)/\sigma^{incl}(\overleftarrow{p}\,)$, as presented in Tables 3 and 4, respectively. Within the errors, r is independent of p_{min} for Al. However, our data indicate a possible decrease of r with increasing p_{min} for Au. Comparing Tables 3 and 4, one can note that the share of the SPA mechanism is noticeably smaller for the subsample with a single pair of protons, i.e. for comparatively peripheral collisions. Probably, for this subsample the dominant role in BPP belongs to other mechanisms, e.g. the spectator type mechanisms suggested in [3] for (anti)neutrino-neon interactions.

Table 3. Contribution from the SPA mechanism

	$\sigma^{SPA}(\overleftarrow{p}\,p)/\sigma^{incl}(\overleftarrow{p}\,)$, %		
target	$p_{min} = 0.25$ GeV/c	$p_{min} = 0.30$ GeV/c	$p_{min} = 0.35$ GeV/c
Al	26.4 ± 4.0	27.0 ± 4.3	24.5 ± 4.4
Au	44.4 ± 5.5	40.2 ± 6.0	34.5 ± 5.7

Table 4. Contribution from the SPA mechanism for the events with one pair of protons

$\sigma^{SPA}(\overleftarrow{p}\,p)/\sigma^{incl}(\overleftarrow{p}\,)$, %	
target	$p_{min} = 0.25$ GeV/c
Al	10.5 ± 4.0
Au	23.5 ± 5.5

The A-dependence of the ratio r at $p_{min} = 0.25$ GeV/c is shown in Fig. 11, where the results of other experiments [6,7,8] obtained under very similar conditions are also presented. The share of the SPA increases with increasing A to become one of the main sources of BPP for heavy nuclei. It can be fitted by a power dependence $\propto A^\beta$, with $\beta = 0.27 \pm 0.05$ (dashed line on Fig. 11).

So far, we have considered SPA with two protons in the final state. This corresponds to subprocesses $\pi^+(pn) \to \overleftarrow{p}\,p$ and $\pi^0(pp) \to \overleftarrow{p}\,p$. Certainly, other subprocesses such as $\pi^+(nn) \to \overleftarrow{p}\,n$, $\pi^0(pn) \to \overleftarrow{p}\,n$ and $\pi^-(pp) \to \overleftarrow{p}\,n$ can occur with a backward produced proton. As estimated in [5] for the case of carbon nuclei, these subprocesses increase the SPA contribution by a factor 1.6 with respect to subprocess (3). Assuming the same factor for Al and Au nuclei, the SPA contribution can, therefore, reach ~40% for Al and ~70% for Au nuclei.

One should also stress that possible rescatterings of the protons produced in subprocess (3) can strongly change their kinematics (including μ^2) and thus lead to an underestimation of the extracted SPA contribution.

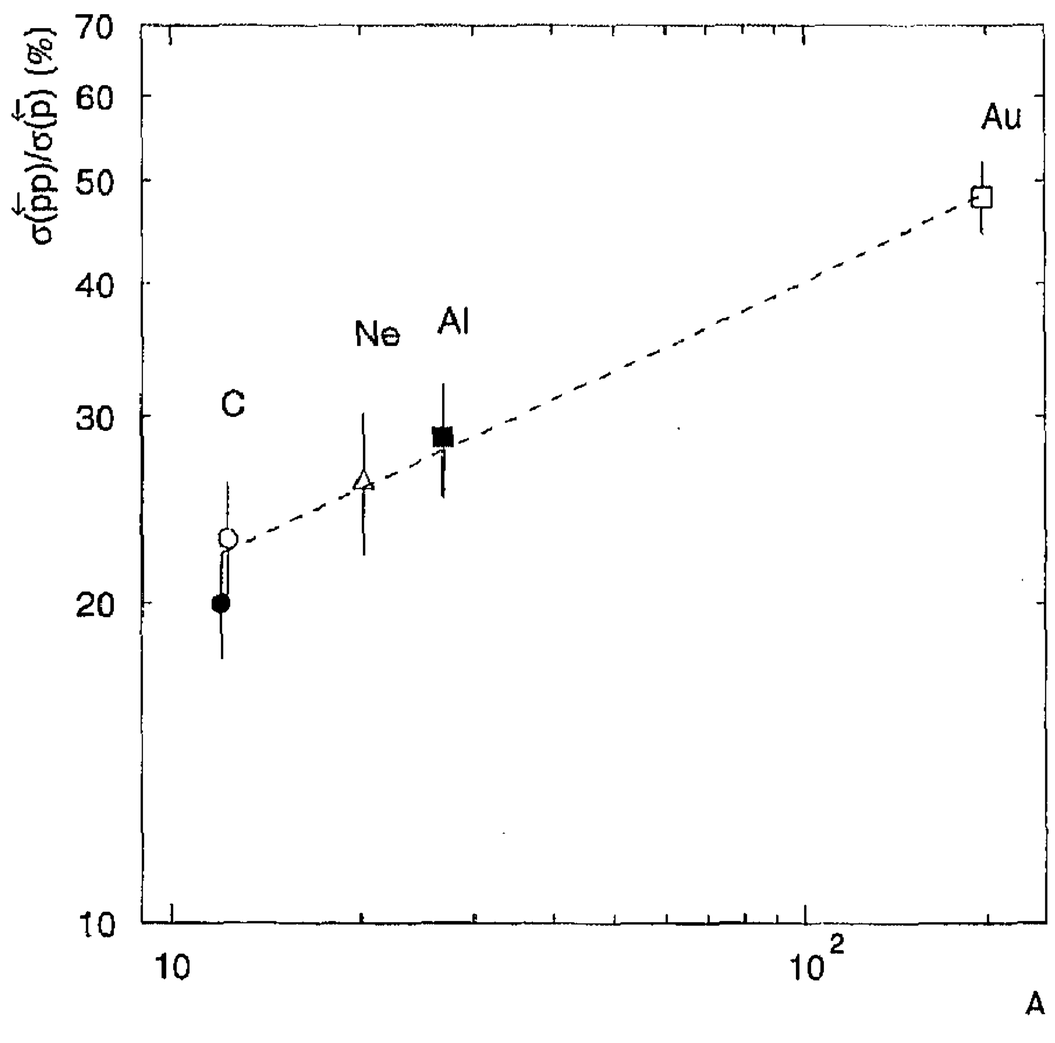

Fig. 11. The contribution of secondary pion absorption to backward proton production, as a function of mass number A. The dashed line corresponds to the best power-law fit (see text)

6 Summary

New experimental data on backward proton production are obtained in (π^+/K^+) Al and (π^+/K^+) Au interactions at 250 GeV/c with the help of the EHS spectrometer. Multiplicity distributions and inclusive spectra of backward protons are measured. The A-dependence of the backward proton yield is consistent with $\propto A^{0.7}$. For Au, the slope parameter of the p_{lab}^2-spectrum increases with increasing emission angle θ_{lab}, but it is, within statistical errors, independent of A.

Semi-inclusive spectra and correlation characteristics of BPP are investigated. From two-proton correlations it is found that a significant part of BPP at $\theta_{lab} > 100^0$ and $p_{lab} > 0.25$ GeV/c, (26±4)% for Al and (44±6)% for Au, can be attributed to secondary pion absorption by a nucleon pair in the nuclear medium, $\pi^+(pn) \rightarrow \overleftarrow{p}\,p$ and $\pi^0(pp) \rightarrow \overleftarrow{p}\,p$. From fitting the contributions of SPA for different nuclei (C, Ne, Al, Au), it is found that the share of the SPA can be described by a power dependence $\propto A^\beta$, with $\beta \approx 0.27 \pm 0.05$. An upper limit of the cross section for the double colour-charge-exchange mechanism of BPP is estimated; the contribution of this mechanism is less than 1% of the high-momentum tail ($p_{lab} > 0.55$ GeV/c) of the inclusive spectrum.

Acknowledgements. It is a pleasure to thank the EHS coordinator L. Montanet and the operating crews and staffs of EHS, SPS and H2 beam, as well as the scanning and processing teams of our laboratories for their invaluable help with this experiment. We are grateful to the III. Physikalisches Institut B, RWTH Aachen, Germany, the DESY-Institut für Hochenergiephysik, Berlin-Zeuthen, Germany, the Department of High Energy Physics, Helsinki University, Finland, and the University of Warsaw and Institute of Nuclear Problems, Poland for early contributions to this experiment. This work is part of the research programme of the "Stichting voor Fundamenteel Onderzoek der Materie (FOM)", which is financially supported by the "Nederlandse Organisatie voor Wetenschappelijk Onderzoek (NWO)". We further thank NWO for support of this project within the program for subsistence to the former Soviet Union (07-13-038).

References

1. A.M. Baldin: Elem. Part. Nucl. 8 (1977) 429.
2. L.L. Frankfurt, M.I. Strikman: Phys. Rep. 76 (1981) 215; ibid. 160 (1988) 235.
3. E. Matsinos et al.: Z. Phys. C44 (1989) 79
4. V.B. Kopeliovich: Sov. J. Nucl. Phys. 43 (1977) 87.
5. M.A. Braun, V.V. Vechernin: Sov. J. Nucl. Phys. 43 (1986) 1016.
6. V.M. Asaturyan, H.R. Gulkanyan, A.G. Khudaverdyan: Sov. J. Nucl. Phys. 45 (1987) 657; Nucl. Phys. A496 (1989) 770.
7. D. Armutlijski et al.: Sov. J. Nucl. Phys. 46 (1987) 1023.
8. M.A. Alimov et al.: Phys. Rev. D46 (1992) 45.
9. V.V. Ammosov et al.: Sov. J. Nucl. Phys. 43 (1986) 759.
10. B.Z. Kopeliovich, F. Nidermayer: Phys. Lett. B117 (1982) 101; JETP 87 (1984) 640.
11. B.Z. Kopeliovich: Sov. J. Part. Nucl. 21 (1990) 49.
12. Ju.M. Antipov et al.: Yad. Fiz. 59 (1993) 157.
13. M. Aguillar-Benitez et al.: Nucl. Instrum. Methods 205 (1983) 79.
14. M. Adamus et al., NA22: Z. Phys. C32 (1986) 475.
15. M. Adamus et al., NA22: Z. Phys. C39 (1988) 311.
16. M. Adamus et al., NA22: Z. Phys. C42 (1989) 377.
17. N.M. Agababyan et.al., NA22: Z. Phys. C56 (1992) 371.
18. N.M. Agababyan et.al., NA22: Z. Phys. C52 (1991) 231.
19. N.A. Nikiforov et.al.: Phys. Rev. C22 (1980) 700.
20. Y.D. Bayukov et al.: Phys. Rev. C20 (1979) 764.
21. V.B. Gavrilov, G.A. Leksin: Deep inelastic nuclear reactions and some aspects of QCD, Preprint ITEP No.128 (1989), Moscow
22. M. Dayon et al.: Z. Phys. C56 (1992) 391
23. K.V. Alanakyan et al.: Sov. J. Nucl. Phys. 25 (1977) 292; ibid. 26 (1977) 539.
24. R.O. Avakyan et al.: Sov. J. Nucl. Phys. 33 (1981) 192.
25. G. Jones: $NN \rightarrow \pi d$ and $NN \rightarrow NN$; a review of experimental results, Vancouver,1981,p.22 (Preprint/ University of British Columbia. TRI-PP-81-62).
26. I.G. Aznauryan, I.A. Troshenkova: Sov. J. Nucl. Phys. 43 (1986) 219.
27. A.S. Goldhaber: Phys. Lett. 53B (1974) 306.
28. J.Boswell et al.: Phys. Rev. C25 (1982) 2540.
29. H. Yokota et al.: Phys. Rev. Lett. 157 (1986) 807.